

## EQUILIBRIUM MOLECULAR DYNAMICS STUDY OF PHONON THERMAL TRANSPORT IN NANOMATERIALS

*Zhanrong Zhong, Xinwei Wang, and Jun Xu*

*Department of Mechanical Engineering, Walter Scott Engineering Center,  
The University of Nebraska—Lincoln, Lincoln, Nebraska, USA*

*In this work, the thermal conductivity of nanofilms, nanowires, and nanoparticles are studied using molecular dynamics simulation. It is found that their thermal conductivity depends significantly on the characteristic size until it reaches a large value. Comparison with results of the lattice Boltzmann method reflects strong effects of surface structure, especially when the film thickness is comparable to the mean free path of phonons. Study of the phonon thermal transport in nanowires and nanoparticles reveals much stronger boundary-scattering effect on thermal transport than in nanofilms, which is attributed to the more confined phonon movements in these two- and one-dimensional nanomaterials.*

### 1. INTRODUCTION

In the past decade, much attention has been attracted to the thermal transport in nanoscale materials. Due to the strong boundary scattering of energy carriers (phonons and electrons), the thermal transport in nanomaterials can be reduced substantially. Many experimental techniques have been developed to investigate the thermal transport in nanomaterials. Examples of these techniques include the  $3\omega$  method for measuring the thermal conductivity of dielectric films [1, 2] and silicon films [3], the photo-thermal reflectance method [4], and the photo-acoustic technique [5].

As for the theoretical study, the method based on the Boltzmann transport equation (BTE) has become a powerful technique and has been used by many researchers. It has been extensively applied to study thermal transport in dielectric materials [6, 7]. In the BTE method, physical understandings of heat transfer and phonon scattering are needed, such as the velocity and relaxation time of energy carriers. On the other hand, it is hard to know the physical properties in some cases, which makes it difficult to capture the structural effect on thermal transport.

Received 1 December 2003; accepted 23 April 2004.

Support for this work from the National Science Foundation (CTS: 0210051), from the University of Nebraska—Lincoln (UNL) through the Faculty Seed Grant, and from the College of Engineering and Technology and the Department of Mechanical Engineering at UNL through the start-up fund are gratefully acknowledged.

Address correspondence to Xinwei Wang, Department of Mechanical Engineering, N104 Walter Scott Engineering Center, The University of Nebraska—Lincoln, Lincoln, NE 68588-0656, USA. E-mail: xwang3@unl.edu

### NOMENCLATURE

$a$	lattice constant	$r_{\text{cut}}$	cutoff distance
$c$	sound velocity	$r_0$	distance between nearest atoms
$c_v$	specific heat	$t$	time
$C_v$	$\rho \cdot c_v$	$\Delta t$	time step
$E$	total energy of an atom	$T$	temperature
$\delta E^2$	fluctuation of $E^2$	$u$	potential energy
$F$	interaction force	$\delta u^2$	fluctuation of $u^2$
$k$	thermal conductivity	$v$	velocity of the atom
$k_B$	Boltzmann's constant	$V$	volume
$k_0$	thermal conductivity of bulk material	$x, y, z$	coordinate directions
$L$	thickness of the film	$\varepsilon$	LJ well depth parameter
$L_0$	mean free path of phonons	$\rho$	density
$m$	atomic mass	$\sigma$	LJ equilibrium separation
$N$	number of atoms; number density of atoms	$\tau$	phonon relaxation time
$P$	probability of atomic velocity distribution	$\phi$	LJ 12-6 potential
$q$	heat flux	<b>Subscripts</b>	
$q_F$	heat flux in the Fourier law	$i, j$	index of the atom
$r$	position of the atom	$m$	index of the direction
		NVT	system with constant atomic number, volume, and temperature

Molecular dynamics (MD) simulation, which directly simulates the trajectory of each atom/molecule in the system, does not have the limitation of the BTE method and becomes more popular. In the 1950s, MD simulation was first applied to calculate the inharmonic one-dimensional chains of atoms [8]. Early work on MD simulation was carried out by Alder et al. [9], Gibson et al. [10], and Rahman [11]. The MD technique has been applied to liquids and gases, giving reasonable results [12–14] and determining the phonon spectra and nanoscale solid structure [15–17]. Work has also been done in studying the thermal conductivity of materials [18, 19]. Recently, Lukes et al. [20] used MD simulation to study the thermal conductivity of solid thin films, showing that the thermal conductivity decreased as film thickness was reduced. Using MD simulation, Volz and Chen [21] investigated the thermal conductivity of silicon nanowires and found that the simulated thermal conductivity was about two orders of magnitude smaller than that of bulk silicon crystals. They also studied the thermal conductivity of silicon crystals and the effect of the domain size and boundary conditions [22]. To date, little MD work has been reported on studies of the anisotropic nature of the thermal transport in nanofilms and nanowires. For nanoparticles, little research has been conducted to address the effect of boundary phonon scattering on thermal transport.

In this article, MD simulation is employed to study the phonon thermal transport in nanofilms, nanoparticles, and nanowires, which have strong phonon scattering at boundaries. For nanofilms and nanowires, the thermal conductivities in all the three directions are reduced by boundary scattering while they show some anisotropic nature. The results indicate a strong reduction of thermal transport in the constrained direction compared with that in the unconstrained direction. In addition to thermal conductivity, the relaxation time of phonons in thin films is studied as

well using three methods. The values of the phonon relaxation time obtained from the three methods deviate slightly, while the trends of variation with the thickness are the same.

## 2. METHODOLOGIES

### 2.1. Basis of the MD Technique

Argon crystal is chosen as the material under study for the reason of simplicity of computation while the fundamental physical phenomena can still be captured. The basis of the MD simulation is to solve the Newtonian equations to obtain the position, force, and velocity of each atom in the system. Each atom has the following movement equation:

$$m_i \frac{d^2 r_i}{dt^2} = \sum_{i \neq j}^N F_{ij} \quad (1)$$

where  $m_i$  is the mass and  $r_i$  is the position of atom  $i$ , and  $N$  is the total number of atoms in the system.  $F_{ij}$  is the interaction force between atoms  $i$  and  $j$ , which can be obtained from the Lennard-Jones (LJ) 12-6 potential [12]:

$$\phi_{ij}(r_{ij}) = 4\varepsilon \left[ \left( \frac{\sigma}{r_{ij}} \right)^{12} - \left( \frac{\sigma}{r_{ij}} \right)^6 \right] \quad (2)$$

$$F_{ij} = -\frac{\partial \phi_{ij}}{\partial r_{ij}} = -\frac{4\varepsilon}{r_{ij}} \left[ 12 \left( \frac{\sigma}{r_{ij}} \right)^{12} - 6 \left( \frac{\sigma}{r_{ij}} \right)^6 \right] \quad (3)$$

where  $\phi_{ij}$  is the LJ potential between two atoms,  $\varepsilon$  is the LJ well depth,  $\sigma$  is the equilibrium separation parameter, and  $r_{ij}$  is the distance between two atoms ( $r_{ij} = r_i - r_j$ ). When  $r_{ij}$  is much larger than  $\sigma$ , the two terms in the potential will become very small. In our calculation, we adopt a widely used cutoff distance,  $r_{\text{cut}} = 2.5\sigma$  [23]. When the distance between two atoms is larger than the cutoff distance, the force will not be considered, which will greatly reduce the computational time.

To solve Eqs. (1)–(3), various methods can be applied. In our program, we adopt one of the widely used Verlet algorithms, in which the half-step leapfrog scheme is used. This algorithm can be expressed as [12]

$$v_i \left( t + \frac{\Delta t}{2} \right) = v_i \left( t - \frac{\Delta t}{2} \right) + \frac{F_{ij}(t)}{m_i} \Delta t \quad (4a)$$

$$r_i(t + \Delta t) = r_i(t) + v_i \left( t + \frac{\Delta t}{2} \right) \Delta t \quad (4b)$$

$$F_{ij}(t + \Delta t) = -\frac{\partial \phi_{ij}(t + \Delta t)}{\partial r_{ij}(t + \Delta t)} \quad (4c)$$

$$v_i(t) = \frac{v_i(t + \Delta t/2) + v_i(t - \Delta t/2)}{2} \quad (4d)$$

where  $v_i$  is the velocity of atom  $i$ , and  $\Delta t$  is the time step, which should be chosen to be much smaller than the phonon relaxation time. In our calculation, we choose  $\Delta t$  as 5 fs, which is much smaller than the typical value of the relaxation time of phonons ( $\sim 1$  ps) in this work.

## 2.2. Thermal Equilibrium Calculation

Before studying thermal transport, the system should be in equilibrium state with the minimum value of potential energy. The temperature is calculated using the kinetic energy of the system, which can be written as [19]

$$T = \frac{\sum_{i=1}^N \frac{1}{2} m v_i^2}{\frac{3}{2} N k_B} \quad (5)$$

where  $k_B (= 1.38 \times 10^{-23} \text{ J/K})$  is Boltzmann's constant.

In this work, we set the initial temperature as 30 K, which can keep the argon crystal in solid state. The distance between nearest neighboring atoms is dependent on temperature, which can be expressed using the following expression [24]:

$$\begin{aligned} \frac{r_0(T)}{\sigma} = & 1.0964 + 0.054792 \left( \frac{k_B T}{\varepsilon} \right) + 0.014743 \left( \frac{k_B T}{\varepsilon} \right)^2 + 0.083484 \left( \frac{k_B T}{\varepsilon} \right)^3 \\ & - 0.23653 \left( \frac{k_B T}{\varepsilon} \right)^4 + 0.25057 \left( \frac{k_B T}{\varepsilon} \right)^5 \end{aligned} \quad (6)$$

where  $r_0$  is the nearest distance between atoms. For the face-centered cubic (fcc) crystal structure studied here, the lattice parameter  $a$  has the form  $a = \sqrt{2} r_0$ . When temperature is chosen as 30 K, the lattice constant  $a$  is equal to 0.5355 nm.

To reach the thermal equilibrium state in an efficient manner, we initialize the velocities of atoms with the Maxwellian distribution [23]:

$$P(v) = 4\pi v^2 \left( \frac{m}{2\pi k_B T} \right)^{3/2} e^{-mv^2/2k_B T} \quad (7)$$

where  $P(v)$  is the density of probability for an atom moving with a velocity  $v$ .

## 2.3. Calculation of Thermal Conductivity

In traditional heat transfer, the heat flux can be calculated using Fourier's law of heat conduction as [19]

$$q_F = -k \cdot \nabla T \quad (8)$$

where  $q_F$  is the heat flux and  $k$  is the thermal conductivity. This equation represents the relationship between  $q_F$  and the temperature gradient only when the time scale is much greater than the phonon relaxation time. When a temperature gradient is

suddenly established, in the very beginning the heat flux  $q$  evolves according to the relaxation law [25, 26]

$$\frac{dq}{dt} = \frac{q_F - q}{\tau} \quad (9)$$

where  $\tau$  is the relaxation time of phonons. For the equilibrium MD simulation conducted in this work, the heat flux  $q_F$  is zero, because there is no macro-temperature gradient in the sample. For this reason, the heat flux  $q$  in Eq. (9) can be written as

$$q_m(t) = q_m(0) \exp\left(\frac{-t}{\tau}\right) \quad (10)$$

where  $q_m(t)$  is the heat flux in the  $m$  ( $m = x, y, z$ ) direction.  $q_m(0)$  is the heat flux at a certain instant and is not zero, due to the statistical oscillation of the system around its equilibrium state. As a result, the time autocorrelation function of the heat flux can be expressed as

$$\langle q_m(0)q_m(t) \rangle = \langle q_m(0)q_m(0) \rangle \exp\left(\frac{-t}{\tau}\right) \quad (11)$$

Furthermore, the Green-Kubo expression of the thermal conductivity, which is related to the long-time autocorrelation function, is given as [19]

$$k_m = \frac{V}{k_B T^2} \int_0^\infty \langle q_m(0)q_m(t) \rangle dt \quad (12)$$

where  $V$  is the volume of the system.

From the equation of energy conservation,

$$\frac{1}{V} \frac{\partial E}{\partial t} + \nabla \cdot \mathbf{q} = 0 \quad (13)$$

and the energy of an atom in terms of the atomic kinetic and potential energies,

$$E_i = \sum_{j=1}^N \frac{1}{2} \phi_{ij} + \frac{1}{2} m v_i^2 \quad (14)$$

we can write the expression of heat flux  $q$  as

$$\begin{aligned} q_m V &= \sum_{i=1}^N v_{im} E_i + \sum_{i=1}^N r_{im} \cdot \frac{1}{2} \cdot \sum_{j=1}^N F_{ijm} (v_{im} + v_{jm}) \\ &= \sum_{i=1}^N v_{im} E_i + \frac{1}{2} \sum_{i=1}^N r_{ijm} \cdot \sum_{j=1}^N F_{ijm} v_{im} \\ &= \sum_{i=1}^N v_{im} E_i + \frac{1}{2} \sum_{i=1}^N \sum_{j>i}^N r_{ijm} \cdot F_{ijm} (v_{im} + v_{jm}) \end{aligned} \quad (15)$$

### 3. RESULTS AND DISCUSSION

#### 3.1. Thermal Transport in Nanofilms

In this section, thermal transport in nanofilms of different thicknesses is studied. The nanofilms studied consist of 20 fcc unit cells in the  $x$  and  $y$  directions, and 2 to 64 fcc unit cells in the  $z$  direction. Periodical boundary conditions are applied to the  $x$  and  $y$  directions, and free boundary conditions to the  $z$  direction. The total computational time is 2 ns for thermal conductivity calculation. The parameters used in the calculation are listed in Table 1.

Figure 1 shows the lattice structure in the  $x$ - $z$  plane for a nanofilm of 8 cells ( $\sim 4.28$  nm) in the  $z$  direction after it reaches the thermal equilibrium state. It is evident that atoms are regularly located around their equilibrium positions, reflecting the crystal structure in the film. At the top and bottom surfaces, however, a few atoms are not so regular because of the free boundary conditions.

**3.1.1. Thermal conductivity.** Figure 2 presents the evolution of the heat flux autocorrelation function for the nanofilm shown in Figure 1. The autocorrelation function becomes close to zero when the time reaches 3 ps for the  $z$  direction and 6 ps for the  $x$  and  $y$  directions. This indicates that phonon transport in the  $z$  direction experiences stronger scattering and relaxation than in the  $x$  and  $y$  directions. The first part of the curves looks exponential, which is consistent with the prediction of Eq. (11). However, there are some vibrations in the long-time part, which take a long time to eliminate. It needs to be pointed out that the autocorrelation function  $\langle q(0)q(t) \rangle$  shown in Figure 2 is averaged over a large time span of 2 ns, which is intended to smooth out the oscillation in the curve. After this long-time calculation, the oscillation of the curve is weak and has negligible effect on the integration of  $\langle q(0)q(t) \rangle$  over time.

Figure 3 shows the thermal conductivity in three directions for the nanofilm of 4.28 nm thickness (shown in Figure 1). The curves indicate that the thermal conductivity in the  $z$  direction is much smaller than those in the  $x$  and  $y$  directions. This is caused by the small size and free boundary conditions in the  $z$  direction, which introduce phonon confinement and diffuse relaxation of phonons at the boundary. Figure 3 demonstrates that a computational time of 2 ns is sufficient to give a converged thermal conductivity.

**Table 1.** Values of parameters used in the calculation

Parameter	Value
LJ well depth parameter, $\epsilon$	$1.653 \times 10^{-21}$ J
LJ equilibrium separation, $\sigma$	3.406 Å
Argon atomic mass, $m$	$6.63 \times 10^{-26}$ kg
Boltzmann constant, $k_B$	$1.38 \times 10^{-23}$ J/K
Lattice constant, $a$	5.355 Å
Cutoff distance, $r_{\text{cut}}$	8.515 Å
Temperature, $T$	30 K
Size of the sample— $x$	10.71 nm
Size of the sample— $y$	10.71 nm
Size of the sample— $z$	1.071–34.272 nm
Time step, $\Delta t$	5 fs

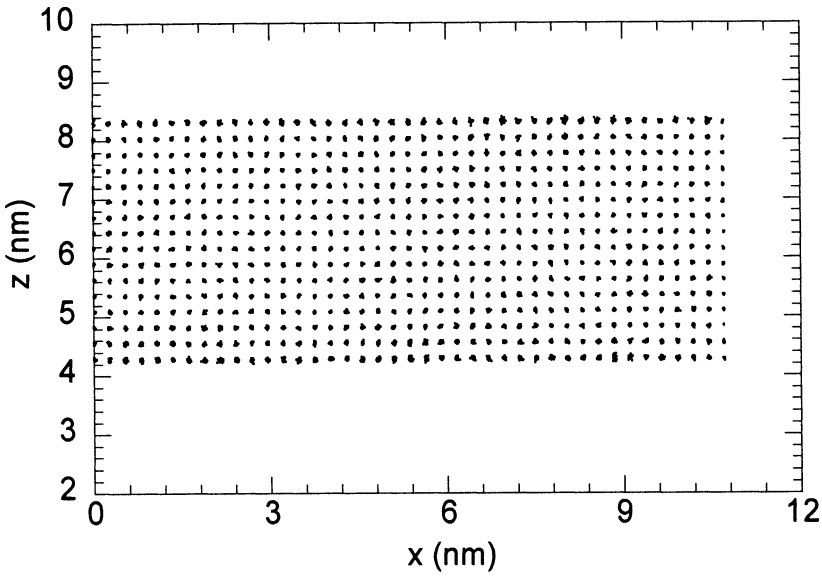


Figure 1. Lattice structure in the  $x$ - $z$  plane for a nanofilm 4.28 nm thick in the  $z$  direction.

In this section, we calculate the thermal conductivities in the  $x$ ,  $y$ , and  $z$  directions for films of different thicknesses. The relationship between the thermal conductivities in the three directions and the thickness of nanofilms is shown in Figure 4. It is observed that the thermal conductivities in the  $x$ ,  $y$ , and  $z$  directions

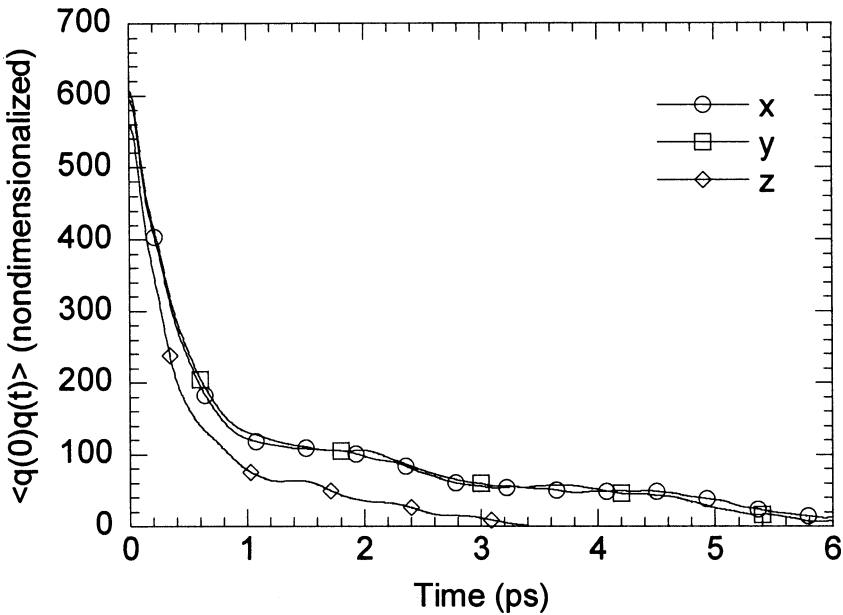


Figure 2. Evolution of heat flux autocorrelation function for the nanofilm of 4.28 nm thickness.

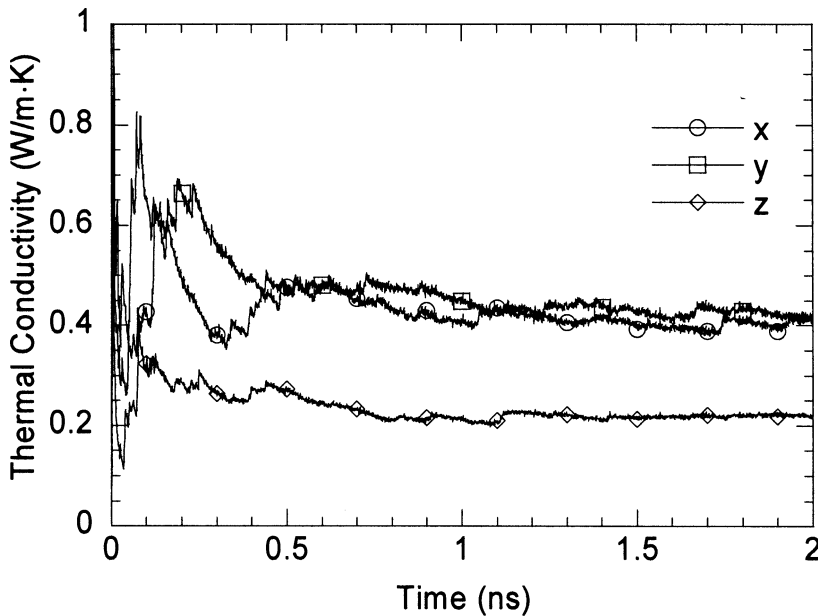


Figure 3. Thermal conductivities in the three directions for the nanofilm of 4.28 nm thickness.

decrease with the decreasing thickness of the film. This reflects the fact that boundary scattering at the top and bottom surfaces introduce diffuse phonon relaxation in the three directions. The thermal conductivity in the  $z$  direction is more affected by the thickness, which is caused by the smaller size and the free boundary condition applied in this direction. When the thickness is comparable to the mean free path of phonons ( $\sim 1.5$  nm as calculated latter), the thermal conductivity in the  $z$  direction varies significantly with thickness, due to the strong boundary scattering. After the thickness reaches large values, the portion of phonons experiencing boundary scattering becomes much smaller. As a result, the thermal conductivity tends to be constant and becomes close to the values in the  $x$  and  $y$  directions. The thermal conductivity at large film thicknesses is around 0.55 W/m K, which is close to the measured thermal conductivity of argon crystal at 30 K, 0.78 W/m K [27]. The difference between them could be attributed to the potential used for argon crystal, which is very appropriate for liquid argon. From this figure, it is evident that the thermal conductivity in the  $x$  and  $y$  directions is also affected by the thickness, which is caused by the diffuse boundary scattering of phonons. It demonstrates that the diffuse scattering of phonons at the top and bottom surfaces of thin films not only reduces the thermal conductivity in the thickness direction, but also reduces the in-plane thermal conductivity. When the thickness of the film becomes smaller, the surface area-to-volume ratio, which is proportional to the inverse of the film thickness, becomes larger. This means that a larger portion of phonons will experience diffuse surface scattering, making their mean free path in the  $x$  and  $y$  directions smaller. Therefore, like the thermal conductivity in the  $z$  direction, the thermal conductivity in the  $x$  and  $y$  directions also becomes smaller when the film thickness decreases.

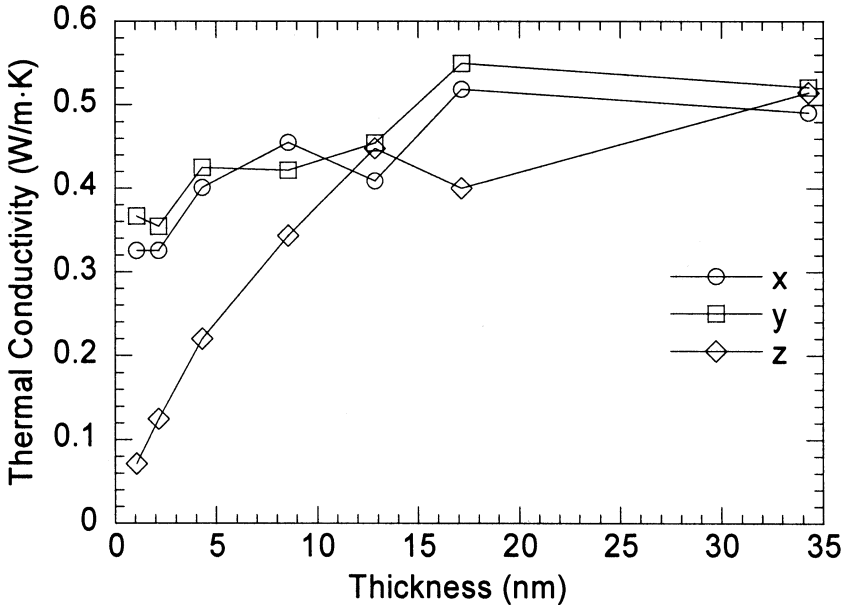
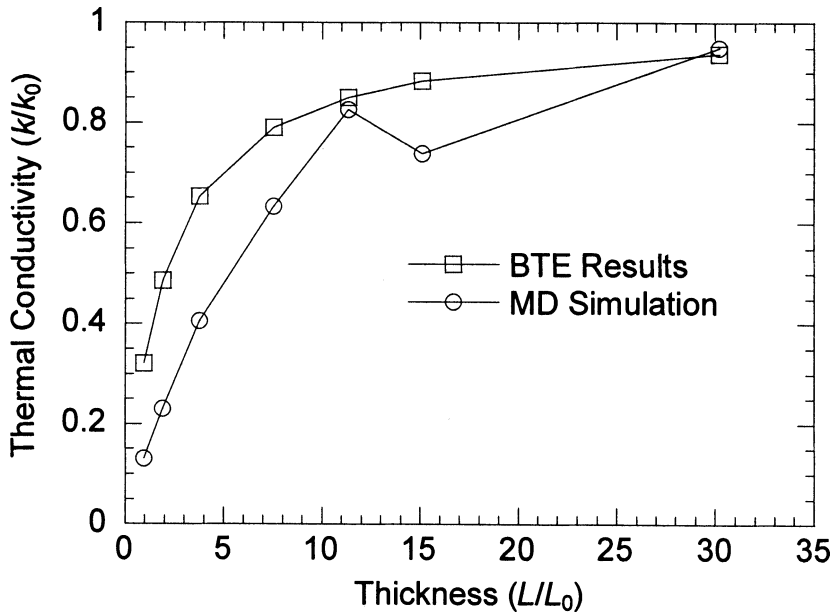


Figure 4. Thermal conductivities of nanofilms versus their thickness.

For the thermal conductivity in the thickness direction of thin films, Figure 5 presents a comparison between the results of MD simulation and those of the Boltzmann transport equation, which has the form [6]

$$\frac{k}{k_0} = \frac{1}{1 + \alpha(L_0/L)} \tag{16}$$

Recently, by solving the BTE using the lattice Boltzmann method (LBM), Xu [28] stated that  $\alpha$  was equal to 2.0. When using Eq. (16), the mean free path of phonons is estimated as  $L_0 = 3k_0/(\rho c_v c)$ , where  $k_0$  is the thermal conductivity of bulk argon,  $c_v$  is the specific heat, and  $c$  is the speed of sound in argon. A close look at Figure 4 reveals that when the thickness reaches 34.27 nm, the thermal conductivity is almost constant. We estimate that the thermal conductivity at 34.27 nm thickness is about  $0.95k_0$ , based on the curve trend.  $c_v$  is calculated using the MD simulation and is detailed in Section 3.1.2. The speed of sound in argon crystal is taken as 1,518 m/s in the [100] direction (thickness direction) at 30 K [29]. Figure 5 demonstrates that the variation trends predicted by the MD simulation and the LBM are close. It is found that the thermal conductivity predicted by MD simulation for thin films is smaller than those predicted by the BTE method, which could be attributed to the loose intermolecular bonding at the top and bottom boundaries, which is not taken into account in the LBM. The other possible reason for the difference between the MD simulation and the LBM is that when solving the BTE using the LBM, only one thermal relaxation time (mean free path) is used. On the other hand, it is evident in Figure 2 that the thermal relaxation time of phonons has a wide span (discussed in Section 3.1.2), which complicates the boundary scattering



**Figure 5.** Comparison of the thermal conductivity in the thickness direction of thin films for MD simulation and the BTE method.  $k_0$  is the thermal conductivity of bulk materials,  $L$  is the film thickness, and  $L_0$  is the mean free path of phonons in bulk materials.

effects and is not accounted for in the LBM. When the phonon movement is solved using the LBM, diffuse boundary scattering is assumed. This boundary condition may not hold true for the MD simulation conducted in this work and will introduce difference between the MD and LBM results.

**3.1.2. Relaxation time of phonons.** In this work, three methods are employed to determine the relaxation time of phonons based on the MD simulation results.

In the first method, by substituting Eq. (11) into Eq. (12) and conducting the integration, we obtain the following equation for the phonon relaxation time:

$$\tau = \frac{k \cdot k_B \cdot T^2}{\langle q(0)q(0) \rangle V} \quad (17)$$

In the second method, it is evident that Eq. (11) proposes an exponential evolution of the autocorrelation function of the heat flux. Since our results give the values of  $\langle q(0)q(t) \rangle$  at each time step, the phonon relaxation time  $\tau$  can be obtained by curve-fitting of  $\langle q(0)q(t) \rangle$  using the exponential function.

In the third method, according to the simplified kinetic theory of heat transfer by phonons, the relaxation time  $\tau$  can also be determined from the calculated thermal conductivity  $k$  with the following equation [19]:

$$\tau = \frac{3k}{\rho c_v c^2} \quad (18)$$

where  $c$  is the sound velocity,  $\rho$  is the density of argon crystal, and  $c_v$  is the specific heat, which can be determined by the fluctuations in the total energy [12],

$$k_B T^2 C_v = \langle \delta E^2 \rangle_{NVT} \tag{19}$$

where  $C_v = \rho c_v$ . The fluctuations in the total energy are divided into uncorrelated kinetic and potential parts,

$$\langle \delta E^2 \rangle_{NVT} = \frac{3}{2} N (k_B T)^2 + \langle \delta u^2 \rangle_{NVT} \tag{20}$$

where

$$\langle \delta u^2 \rangle_{NVT} = \langle u^2 \rangle_{NVT} - \langle u \rangle_{NVT}^2 \tag{21}$$

in which  $u$  is the potential energy and  $N$  is the number density of atoms. Figure 6 presents the time evolution of the specific heat of the thin film 8.57 nm thick. At the beginning, the curve of specific heat displays some vibration due to the vibration of the system energy. After 1.0 ns, it tends to be constant, which can be used to determine the phonon relaxation time.

Figure 7 shows an example of the process to estimate the phonon relaxation time in the  $z$  direction by the curve-fitting method for a film of 8.57 nm thickness. We found that the exponential curve fitting applies only to the early part of the phonon thermal relaxation process, which is shown in Figure 7. From Figure 2, it is seen that some phonons have much longer relaxation times, which cannot be fitted using a single thermal relaxation time.

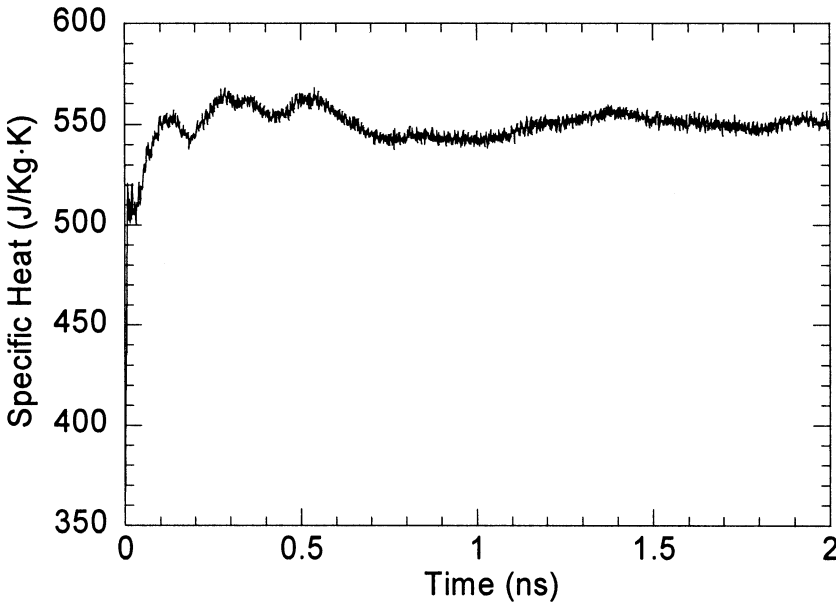


Figure 6. Evolution of the specific heat of the thin film of 8.57 nm thickness.

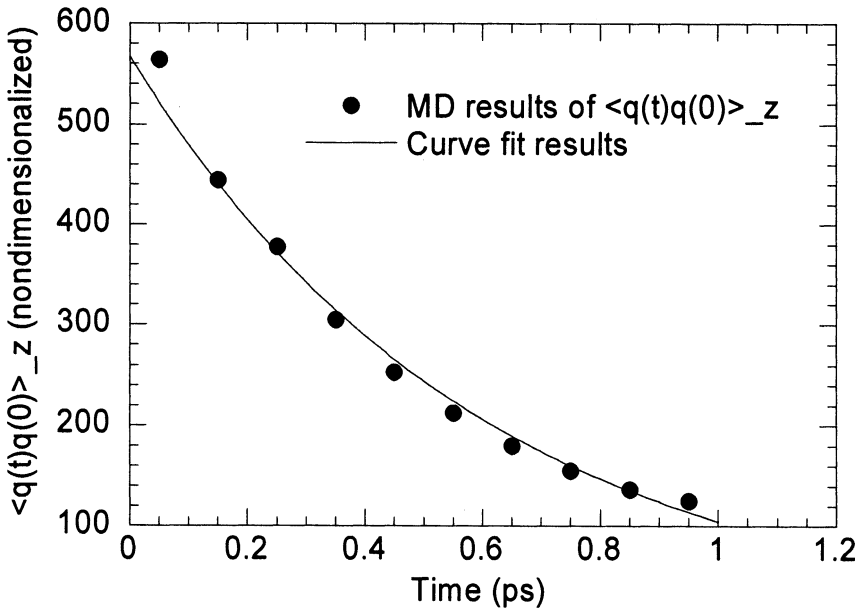


Figure 7. Curve-fitting of  $\langle q(0)q(t) \rangle$  to determine the phonon relaxation time.

The relation between the phonon relaxation time (in the  $z$  direction) and the film thickness is shown in Figure 8. Each curve represents the result using one method as specified in the figure. It indicates that the phonon relaxation time increases with increasing film thickness, meaning less constraint on the movement of phonons in thicker films. When the thickness becomes large enough, the phonon relaxation time tends to be constant. The results obtained using the three methods are not identical, whereas the variation trends are close. When using Eq. (17) to determine the phonon relaxation time, it is assumed that the autocorrelation of heat flux decays with time exponentially. However, Figure 2 shows that this assumption does not hold for the long time period. Therefore, Eq. (17) gives an averaged thermal relaxation time considering both the short- and long-time relaxations. When using curve-fitting to determine the phonon relaxation time, only the short-time thermal relaxation is fitted, while the long-time thermal relaxation is neglected. Therefore, the curve-fitting method predicts a smaller phonon relaxation time as demonstrated in Figure 8. Equation (18) gives another averaged relaxation time for phonons based on the specific heat. It is observed the phonon relaxation time predicted using Eq. (18) is even smaller than the curve-fitting result. In this work, the specific heat  $c_v$  is calculated using free boundary conditions at the top and bottom surfaces, which cannot make the volume constant. Our previous work has proved that this can overpredict the specific heat  $c_v$  to a large extent [30]. As a result, the phonon relaxation time determined using this specific heat is smaller.

### 3.2. Thermal Transport in Nanoparticles and Nanowires

A big benefit of MD simulation is that it can be readily applied to different shapes of nanomaterials. In addition to nanofilms, thermal transport in

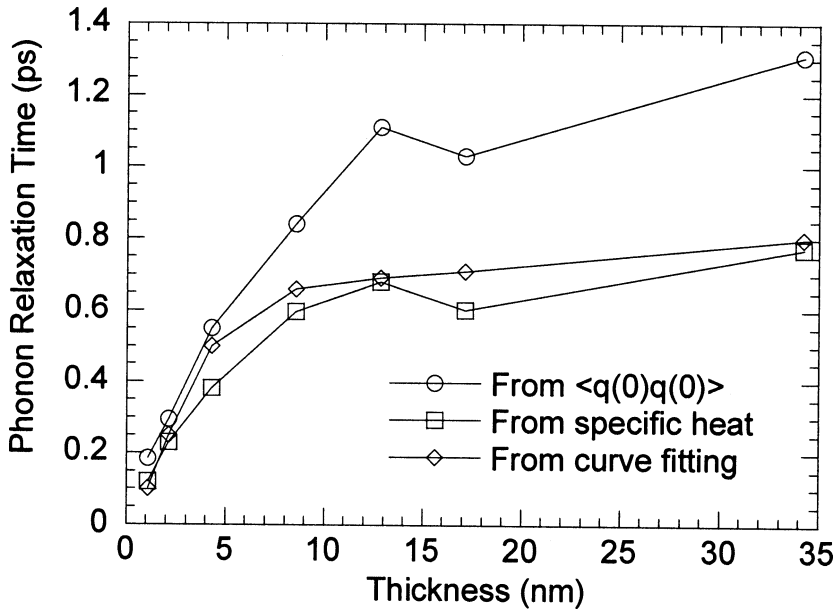


Figure 8. Relaxation time of phonon movement in the  $z$  direction for different film thicknesses.

nanoparticles and nanowires is also studied in this work. Figure 9 shows the lattice structure of a nanoparticle with 8.57 nm diameter. Free boundary conditions are applied to the three directions, which makes the surface a little irregular.

Because of the symmetry of the nanoparticle, the thermal conductivities in the three directions are close to each other. Figure 10 shows the relationship between the thermal conductivities in the  $x$ ,  $y$ , and  $z$  directions and the diameter of nanoparticles. The values of the thermal conductivity are different from those of the nanofilms (detailed in Figure 13), whereas the trend of variation of the thermal conductivity versus the characteristic size of the material is the same. When the diameter becomes large enough, the thermal conductivity tends to be constant. This is because when the diameter of the particle becomes much larger than the mean free path of phonons, the number of phonons experiencing boundary scattering will become negligible in comparison with the total number of phonons in the particle. Therefore, the mean free path of phonons will be close to that of bulk material and independent of the particle size.

Figure 11 shows the lattice structure in the  $x$ - $z$  plane for a nanowire, which is 21.42 nm long in the longitudinal ( $z$ ) direction and 4.28 nm wide (diameter) in the transverse ( $x$  and  $y$ ) directions. Free boundary conditions are applied to the boundaries in the  $x$  and  $y$  directions and periodic boundary conditions to the boundaries in the  $z$  direction. In the computation, it is found that some atoms tend to escape from the system surface because of their high kinetic energy at the free surface of the sample. However, the number of atoms escaping from the sample surface is much smaller than the number of total atoms in the system.

Figure 12 shows the variation of the thermal conductivity in the three directions against the diameter of nanowires. Despite the large domain size in the axial

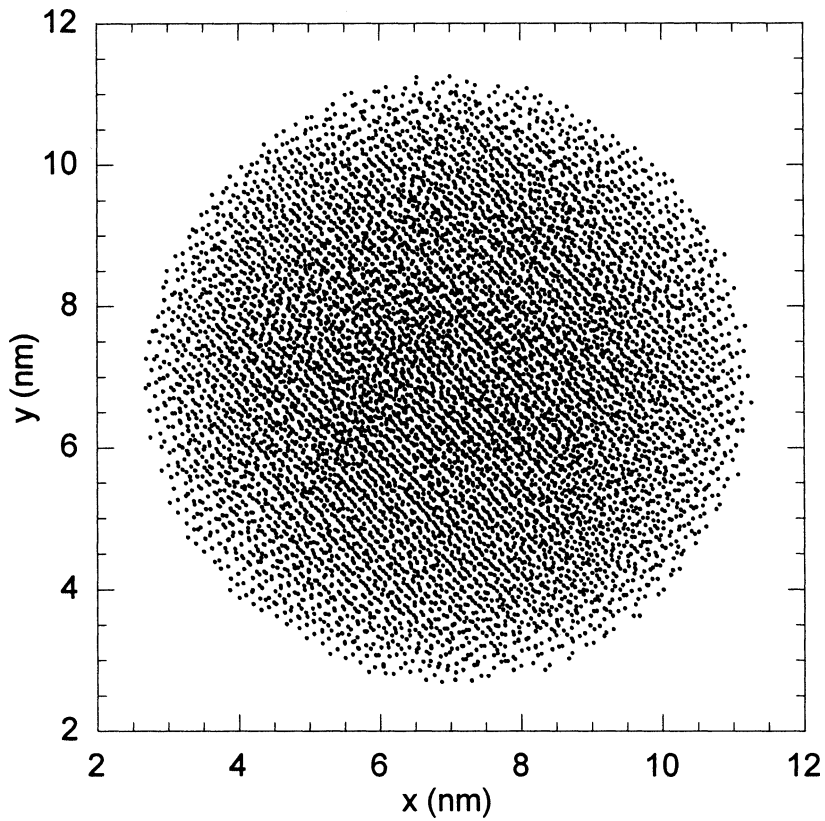


Figure 9. Lattice structure of a nanoparticle with 8.57 nm diameter.

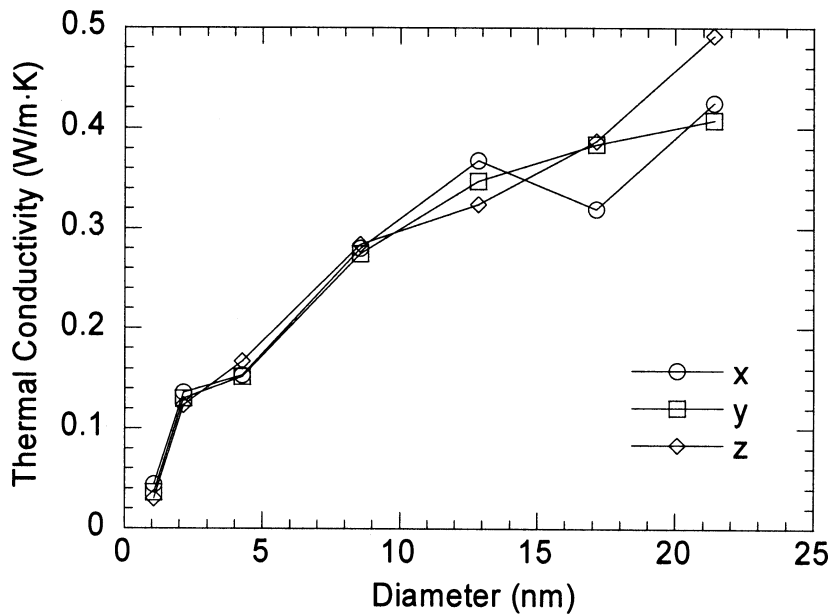
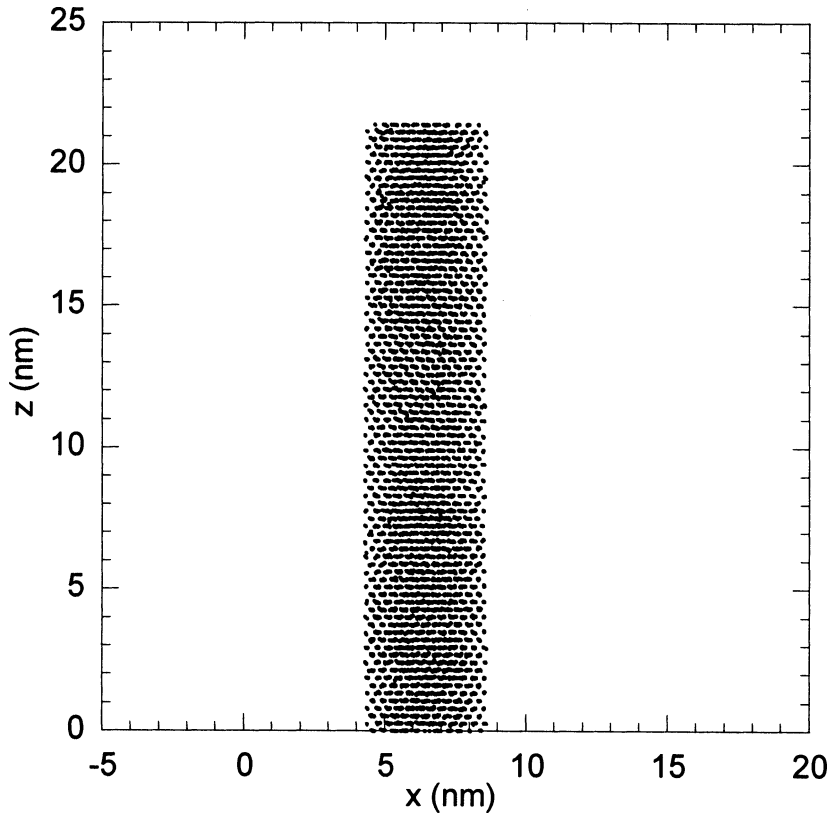


Figure 10. Relation between the thermal conductivities and the diameter of nanoparticles.



**Figure 11.** Lattice structure in the  $x$ - $z$  plane for a nanowire 21.42 nm long and 4.28 nm wide (diameter).

direction ( $z$ ) of the nanowire, the thermal conductivity in this direction is significantly reduced by the phonon scattering at boundaries in the  $x$  and  $y$  directions. It is evident that the phonon boundary scattering reduces the thermal transport more in the  $x$  and  $y$  directions than that in the  $z$  direction. When the diameter is small, the thermal conductivity decreases significantly with decreasing diameter. When the diameter becomes large enough, the thermal conductivity tends to be constant, which is similar to the situations of nanofilms and nanoparticles. This variation trend is also consistent with that of silicon nanowires, which was studied by Volz and Chen [21, 31]. With the same diameter and thickness, the surface area-to-volume ratio of nanowires is about two times that of thin films, so the effect of the diffuse boundary scattering of phonons in nanowires has a much stronger effect on the movement of phonons than that in thin films. Thus, as Figure 12 indicates, the thermal conductivity in the  $z$  direction varies with the diameter much more than the in-plane thermal conductivity of thin films (as Figure 4 indicates).

As a summary, variations of the thermal conductivity in the thickness or diameter direction with the characteristic size of different nanomaterials are compared in Figure 13. It is found that with the same characteristic size, the thermal conductivity of nanofilms is larger than that of nanoparticles and nanowires. The

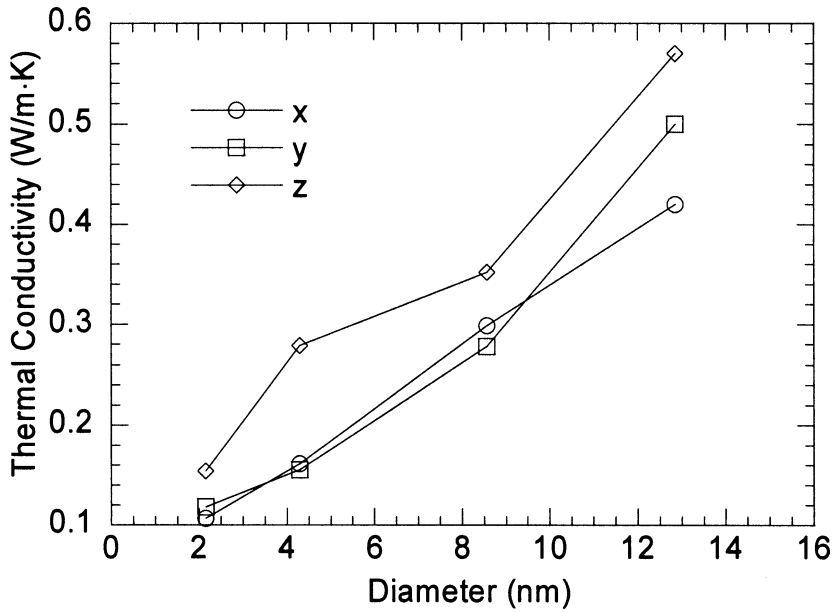


Figure 12. Thermal conductivities of nanowires versus their diameter.

reason is that the portion of phonons experiencing boundary scattering in nanofilms is less than that in nanoparticles and nanowires. It is understandable that with the same diameter, nanoparticles should introduce more boundary scattering than

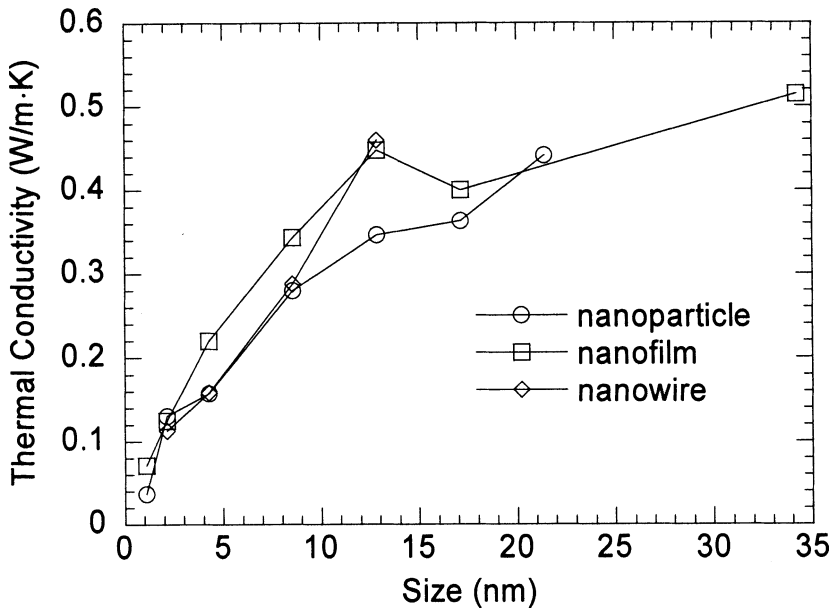


Figure 13. Variations of thermal conductivity versus the characteristic size of different nanomaterials.

nanowires. However, our results show that the difference of this constraint induces marginal difference in the thermal conductivity only when the diameter of nanowires/particles is small.

#### 4. CONCLUSIONS

In this work, thermal conductivities of nanofilms, nanowires, and nanoparticles were studied using equilibrium MD simulation. It was found that the thickness of films and diameter of nanoparticle/wires strongly constrain the movement of phonons by introducing boundary scattering, thereby reducing the thermal conductivity. When the characteristic length becomes large enough, the thermal conductivity tends to be constant. Furthermore, it was found that the thermal conductivity of nanowires in the axial direction and nanofilms in the  $x$  and  $y$  directions was also influenced by the diameter and thickness, which could be attributed to the surface structure and diffuse scattering of phonons at boundaries. We demonstrated that the relaxation time of phonons could be calculated through curve-fitting of the autocorrelation function of heat flux. The autocorrelation function revealed that thermal relaxation could not be simply represented with an exponential function, since a large number of phonons thermally relax with a longer relaxation time.

#### REFERENCES

1. D. G. Cahill and T. H. Allen, Thermal Conductivity of Sputtered and Evaporated SiO<sub>2</sub> and TiO<sub>2</sub> Optical Coatings, *Appl. Phys. Lett.*, vol. 65, pp. 309–311, 1994.
2. S. M. Lee and D. G. Cahill, Heat Transport in Thin Dielectric Films, *J. Appl. Phys.*, vol. 81, pp. 2590–2595, 1997.
3. Y. S. Ju and K. E. Goodson, Phonon Scattering in Silicon Films with Thickness of Order 100 nm, *Appl. Phys. Lett.*, vol. 74, pp. 3005–3007, 1999.
4. K. E. Goodson, O. W. Käding, M. Rösler, and M. Zachai, Experimental Investigation of Thermal Conduction Normal to Diamond-Silicon Boundaries, *J. Appl. Phys.*, vol. 77, pp. 1385–1392, 1995.
5. X. Wang, H. Hu, and X. Xu, Photo-Acoustic Measurement of Thermal Conductivity of Thin Films and Bulk Materials, *J. Heat Transfer*, vol. 123, pp. 138–144, 2001.
6. A. Majumdar, Microscale Heat Conduction in Dielectric Thin Films, *ASME J. Heat Transfer*, vol. 115, pp. 7–16, 1993.
7. G. Chen, Ballistic-Diffusive Heat-Conduction Equations, *Phys. Rev. Lett.*, vol. 86, pp. 2297–2300, 2001.
8. E. Fermi, J. R. Pasta, and S. Ulam, *Collected Papers of Enrico Fermi*, University of Chicago Press, Chicago, 1965.
9. B. J. Alder and T. H. Wainwright, Studies in Molecular Dynamics. II. Behavior of a Small Number of Elastic Spheres, *J. Chem. Phys.*, vol. 33, pp. 1439–1451, 1960.
10. J. B. Gibson, A. N. Goland, M. Milgram, and G. H. Vineyard, Dynamics of Radiation Damage, *Phys. Rev.*, vol. 120, pp. 1229–1253, 1960.
11. A. Rahman, Correlations in the Motion of Liquid Argon, *Phys. Rev.*, vol. 136, pp. A405–411, 1964.
12. M. P. Allen and D. J. Tildesley, *Computer Simulation of Liquids*, chaps 1–4, Clarendon Press, Oxford, 1987.
13. D. J. Evans and G. P. Morris, *Statistical Mechanics of Nonequilibrium Liquids*, Academic Press, London, 1990.

14. Y. H. Lee, R. Biswas, C. M. Soukoulis, C. Z. Wang, C. T. Chan, and K. M. Ho, Molecular-Dynamics Simulation of Thermal Conductivity in Amorphous Silicon, *Phys. Rev. B*, vol. 43, pp. 6573–6580, 1991.
15. T. M. Hakim and H. R. Glyde, Phonons in Solid Argon Monolayers, *Phys. Rev. B*, vol. 41, pp. 1640–1644, 1990.
16. R. Meyer and P. Entel, Martensite-Austenite Transition and Phonon Dispersion Curves of Fe-xNi Studied by Molecular-Dynamics Simulations, *Phys. Rev. B*, vol. 57, pp. 5140–5147, 1998.
17. C. Z. Wang, C. T. Chan, and K. M. Ho, Tight-Binding Molecular-Dynamics Study of Phonon Anharmonic Effects in Silicon and Diamond, *Phys. Rev. B*, vol. 42, pp. 11276–11283, 1990.
18. J. C. Ladd, B. Moran, and W. G. Hoover, Lattice Thermal Conductivity: A Comparison of Molecular Dynamics and Anharmonic Lattice Dynamics, *Phys. Rev. B*, vol. 34, pp. 5058–5064, 1986.
19. S. G. Volz, J. B. Saulnier, M. Lallemand, B. Perrin, P. Depondt, and M. Mareschal, Transient Fourier-Law Deviation by Molecular Dynamics in Solid Argon, *Phys. Rev. B*, vol. 54, pp. 340–347, 1996.
20. J. R. Lukes, X. G. Liang, and C. L. Tien, Molecular Dynamics Study of Solid Thin-Film Thermal Conductivity, *Proc. ASME Heat Transfer Division, HTD-Vol. 361-4*, vol. 4, pp. 229–240, ASME, New York, 1998.
21. S. G. Volz and G. Chen, Molecular Dynamics of Thermal Conductivity of Silicon Nanowires, *Appl. Phys. Lett.*, vol. 75, pp. 2056–2058, 1999.
22. S. G. Volz and G. Chen, Molecular-Dynamics Simulation of Thermal Conductivity of Silicon Crystals, *Phys. Rev. B*, vol. 61, pp. 2651–2656, 2000.
23. X. Wang and X. Xu, Molecular Dynamics Simulation of Heat Transfer and Phase Change during Laser Material Interaction, *ASME J. Heat Transfer*, vol. 124, pp. 265–274, 2002.
24. J. Q. Broughton and G. H. Gilmer, Molecular Dynamics Investigation of the Crystal-Fluid Interface. I. Bulk Properties, *J. Chem. Phys.*, vol. 79, pp. 5095–5104, 1983.
25. C. Cattaneo, Sur une forme de l'équation de la chaleur éliminant le paradoxe d'une propagation instantanée, *C. R. Acad. Sci.*, vol. 247, pp. 431–433, 1958.
26. P. Vernotte, Les paradoxes de la théorie continue de l'équation de la chaleur, *C. R. Acad. Sci.*, vol. 246, pp. 3154–3155, 1958.
27. O. G., Peterson, D. N., Batchelder, and R. O., Simmons, Measurements of X-Ray Lattice Constant, Thermal Expansivity, and Isothermal Compressibility of Argon Crystals, *Phys. Rev.*, vol. 150, pp. 703–711, 1996.
28. J. Xu, Lattice Boltzmann Method for Thermal Transport at Nanoscales and in Ultra-short Time Domains, Master Thesis, University of Nebraska-Lincoln, 2004.
29. G. J. Keeler and D. N. Batchelder, Measurement of the Elastic Constants of Argon from 3 to 77°K, *J. Phys. C: Solid State Phys.*, vol. 3, pp. 510–522, 1970.
30. X. Wang and X. Xu, Molecular Dynamics Simulation of Heat Transfer and Phase Change during Laser Material Interaction, *ASME J. Heat Transfer*, vol. 124, pp. 265–274, 2002.
31. S. G. Volz and G. Chen, Molecular Dynamics Simulation of Thermal Conductivity in Bulk Silicon and Nanowires, *Proc. ASME Heat Transfer Division, HTD-Vol. 361-4*, vol. 4, pp. 199–208, ASME, New York, 1998.

Copyright of Numerical Heat Transfer: Part B -- Fundamentals is the property of Taylor & Francis Ltd and its content may not be copied or emailed to multiple sites or posted to a listserv without the copyright holder's express written permission. However, users may print, download, or email articles for individual use.